Electric Power Systems Research 210 (2022) 108084

Contents lists available at ScienceDirect

Electric Power Systems Research

journal homepage: www.elsevier.com/locate/epsr

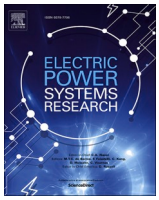

Multivariable phase-locked loop free strategy for power control of grid-connected voltage source converters

Carlos Diaz-Sanahuja, Ignacio Peñarrocha-Alós *, Ricardo Vidal-Albalate

Department of Industrial Systems Engineering and Design, Jaume I University, Castelló 12071, Spain

ARTICLE INFO

Keywords:
VSC
Multivariable control
Anti-windup
PLL
Weak grid

ABSTRACT

A multivariable control strategy in a *dq* reference frame for grid-connected voltage source converters (VSCs) without using a phase-locked loop (PLL) is presented in this paper. First, common VSC controls such as vector current control (VCC) and grid voltage modulated direct power control (GVM-DPC) are analyzed and their main drawbacks are identified. Then, the multivariable control strategy is presented, including the implementation of saturation and anti-windup mechanisms, and limitation of overcurrents. Next, different uncertainty channels that may lead to instability in each approach are analyzed, showing the drawbacks related to the use of a PLL, which are avoided in our proposal. The effectiveness of the three strategies is compared by means of MATLAB/Simulink simulations, showing that the proposal presents a more robust behavior, specially in weak grids.

1. Introduction

The use of grid-connected voltage source converters (VSCs) is increasing fast due to the development of smart grids, flexible AC transmission systems, high-voltage DC systems and renewable energy sources. This poses new challenges to power grids that require advanced control strategies to enhance their integration, performance and robustness [1,2].

Vector current control (VCC) uses a synchronous rotating *dq* frame to transform AC values into DC ones, as well as feedforward terms to decouple the *d* and *q* current control loops, allowing the use of standard single-input single-outpu linear control techniques as proportional-integral (PI) control [3,4]. However, the use of a phase-locked loop (PLL) to get the grid voltage angle can cause a slow transient response, and the interaction between the PLL and the current control loops may cause harmonic problems in weak grids (WG) and even make the system unstable [5–7].

Alternatively, several PLL-free control strategies have been proposed. In [8] uses a stationary frame where variables are sinusoidal, and proportional resonant (PR) controllers are used. The power synchronization control proposed in [9] tries to mimic the operation of a synchronous machine to avoid the PLL. Similarly, Virtual Synchronous Machines avoid the use of PLL by emulating the behavior of synchronous machines [10,11].

Direct power control (DPC) has been widely used as an alternative to VCC [12–14]. Moreover, with the aim of increasing the robustness, sliding-mode control (SMC) and passivity-based control (PBC) DPC have been developed. SMC in [12,13] uses a stationary reference frame in order to achieve an exponential convergence of the tracking error of active and reactive powers. The PBC-DPC in [14] also ensures the exponential stability and uniform performance over all operating points. Both the SMC-DPC and PBC-DPC obtain faster transient response than PI controllers and a robust response against parameter uncertainty, however some ripples in active and reactive powers may appear.

Recently, the grid voltage modulated direct power control (GVM-DPC) was introduced in [15,16] aimed at designing a robust and simple control law to achieve a convergence rate of the instantaneous active and reactive powers and reducing the power ripples and total harmonic distortion (TDH) of the output current in steady-state. It achieves an independent control of the active and reactive powers by changing the variables from a stationary frame into new control variables presented in a *dq* frame without the need of using the synchronous coordinate transformation. Hence, similar to VCC, it uses PI regulators with additional feedforward terms for decoupling and linearizing. Due to the use of simple control laws and good performance, VCC and GVM-DPC are specially interesting approaches. However they present some drawbacks related to the use of a PLL or the use of decoupling terms that difficult the implementation of the control action saturation and anti-windup (AW) mechanisms.

In this work, a MIMO approach in a *dq* rotating frame is proposed, in

* Corresponding author.
E-mail addresses: csanahuj@uji.es (C. Diaz-Sanahuja), ipenarro@uji.es (I. Peñarrocha-Alós).

https://doi.org/10.1016/j.epsr.2022.108084
Received 23 August 2021; Received in revised form 11 March 2022; Accepted 8 May 2022
Available online 17 May 2022

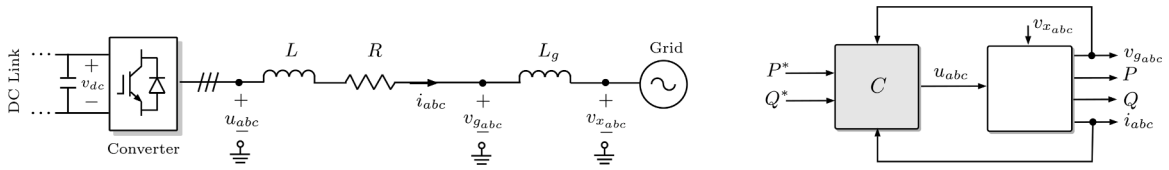

Fig. 1. Model of the system and controller structure.

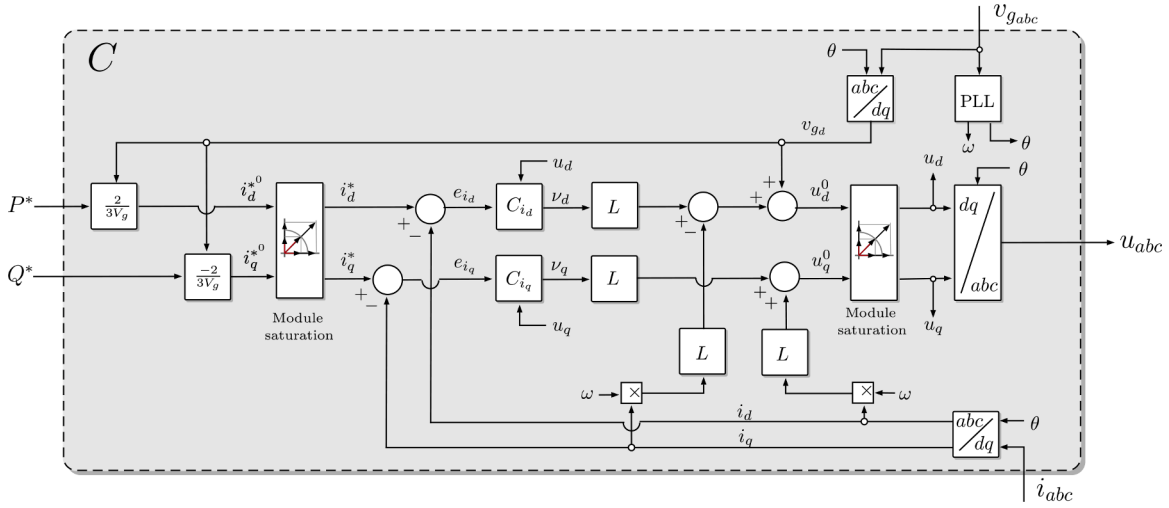

Fig. 2. VCC controller block diagram.

which active and reactive powers are controlled by means of a multivariable state-feedback current controller with reference weighting and considering that the VSC generates its own angle as the integration of a constant angular velocity for the frame transformation (PLL-free). Removing the PLL allows us to directly design the controller without taking into account the coupling dynamics between PLL and current controller, but generates internal oscillating signals to be tracked that we tackle from the controller design. On the other hand, we incorporate and anti-windup multivariable mechanism that allow us to tackle the coupling between integral terms, the presence of weighting factors, and helps us in the synchronization with the grid.

Notation: In this work, subscript *abc* refers to a vector $x_{abc} = [x_a\ x_b\ x_c]^T$, $\alpha\beta$ to a vector $x_{\alpha\beta} = [x_\alpha\ x_\beta]^T$, *dq* to a vector $x_{dq} = [x_d\ x_q]^T$, and *PQ* to a vector $x_{PQ} = [x_P\ x_Q]^T$. The Euclidean norm operator is $\|\cdot\|$, $\mathbf{I}$ and $\mathbf{0}$ are the identity and zero matrices $\in \mathbb{R}^{2\times 2}$, and $\mathbf{J} = [[0\quad 1]^T[-1\quad 0]^T]$.

2. Problem statement

The model of a three-phase VSC connected to the AC grid is shown in Fig. 1. It also shows an overview of the controller C that has to regulate the power delivered to the grid. P^* and Q^* are the active and reactive power references respectively, and the available measurements are the currents i_{abc} and voltages $v_{g_{abc}}$. The controller computes the VSC voltage u_{abc} such that the active and reactive powers delivered to the grid track their references. In order to limit the currents, this controller C has an internal current control whose references come from an outter power controller. In this work, U_{sat} refers the maximum achievable voltage of the converter, I_N is its rated current and V_g denotes the amplitude of $v_{g_{abc}}$. The parameters R and L of the converter are assumed to be known, but not the grid related values (impedance L_g and exogenous voltage v_x). In the sequel, we present alternatives found in the literature to implement this power control.

2.1. Vector current control

Fig. 2 shows the structure of the VCC [17]. First, the grid voltage angle θ is obtained from a PLL [18] using the measurement $v_{g_{abc}}$. Then, $v_{g_{abc}}$ and i_{abc} are transformed to the *dq* frame using θ and Clarke-Park transformations, leading to $v_{g_{dq}}$ and i_{dq} (note that $v_{g_{dq}} = [v_{g_d}\ 0]^T = [V_g\ 0]^T$). With grid voltage and power references $\mathscr{S}^* = [P^*\ Q^*]^T$ the current references i_{dq}^{*0}, are obtained and limited as

$$i_{dq}^{*0} = \frac{2}{3}\mathscr{V}_{dq}{}^{-1}\mathscr{S}^*,\ \mathscr{V}_{dq} = \begin{bmatrix} v_{g_{dq}} & \mathbf{J}^T v_{g_{dq}} \end{bmatrix},$$
$$i_{dq}^* = \begin{cases} i_{dq}^{*0}, & \text{if } \|i_{dq}^{*0}\| \le I_N; \\ \dfrac{I_N}{\|\,i_{dq}^{*0}\|}\, i_{dq}^{*0}, & \text{if } \|\,i_{dq}^{*0}\| > I_N. \end{cases} \tag{1}$$

Control actions u_{dq}^0 are computed with feedforward terms for decoupling *d* and *q* channels and feedback terms as

$$u_d^0 = \underbrace{V_g - L\omega i_q}_{\text{feedforward}} + \underbrace{L\nu_d}_{\text{feedback}},\quad u_q^0 = \underbrace{L\omega i_d}_{\text{feedforward}} + \underbrace{L\nu_q}_{\text{feedback}}, \tag{2}$$

where ν_d and ν_q are determined by the PI controllers C_{i_d} and C_{i_q} defined as

$$C_{i_j}:\quad \nu_j = K_{p,i_j}\left(i_j^* - i_j\right) + K_{i,i_j}\int_0^t \left(i_j^* - i_j\right)d\tau,\quad j = \{d, q\}, \tag{3}$$

where K_{p,i_d} and K_{p,i_q} are the proportional gains, and K_{i,i_d} and K_{i,i_q} are the integral gains. Saturation of the control action is done over the module of the two components of u_{dq} (instead of saturating each component separately that would lead to voltages higher than saturation voltage value) as

$$u_{dq} = \begin{cases} u_{dq}^0, & \text{if } \|\,u_{dq}^0\,\| \le U_{sat}; \\ \dfrac{u_{dq}^0}{\|\,u_{dq}^0\|}\, U_{sat}, & \text{if } \|\,u_{dq}^0\,\| > U_{sat} \end{cases} \tag{4}$$

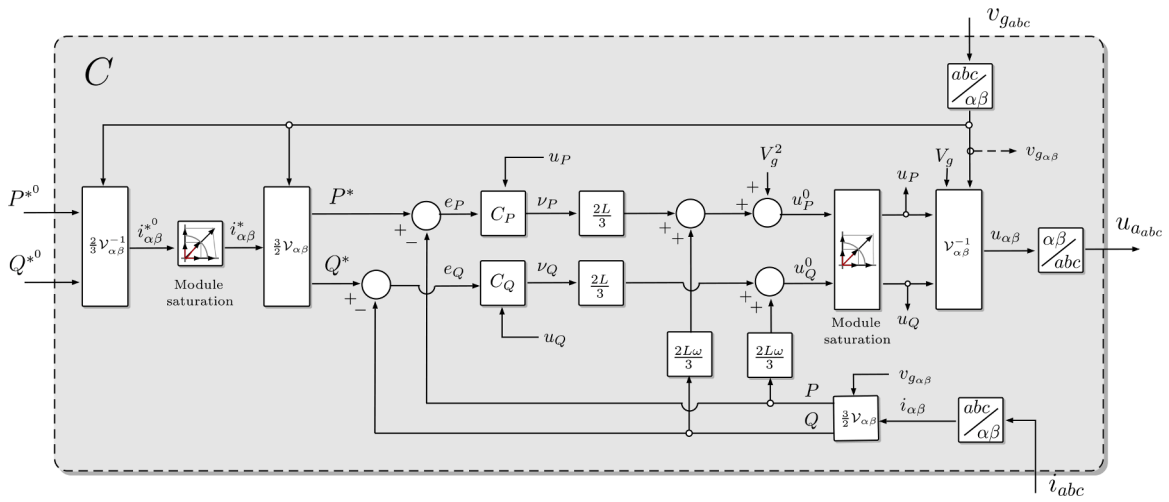

Fig. 3. GVM-DPC controller block diagram.

When the control action satures, both integral terms are frozen. However, each component of u^0_{dq} depends on the two outputs ν_{dq} of the two PI controllers and it is not clear which of them saturates the control action, which is a common drawback when saturating controllers with downstream decoupling terms. Voltage u_{abc} is finally computed from u_{dq} using inverse Clarke-Park transformation.

The controller parameters are designed using the nominal closed-loop (CL) model (i.e., assuming a stiff grid with $L_g = 0$ and no saturations), that presents a decoupled dynamic between d and q, leading to

$$\frac{i_d(s)}{i^*_d(s)} = \frac{K_{p,i_d}\, s + K_{i,i_d}}{s^2 + \left(K_{p,i_d} + \dfrac{R}{L}\right) s + K_{i,i_d}},$$
$$\frac{i_q(s)}{i^*_q(s)} = \frac{K_{p,i_q}\, s + K_{i,i_q}}{s^2 + \left(K_{p,i_q} + \dfrac{R}{L}\right) s + K_{i,i_q}}. \tag{5}$$

The controller gains can be computed to obtain some given CL poles location, for instance, using internal model control [19].

2.2. Grid voltage modulated direct power control

Fig. 3 shows the block diagram of the GVM-DPC approach [15]. Clarke transformations are applied on $v_{g_{abc}}$ and i_{abc} to obtain $v_{g_{\alpha\beta}}$ and $i_{\alpha\beta}$. Then, using the original power references $\mathscr{S}^{*^0} = [P^{*^0}\ Q^{*^0}]^T$ and $v_{g_{\alpha\beta}}$, the equivalent current references $i^{*^0}_{\alpha\beta}$ are obtained and saturated in modulus as

$$i^{*^0}_{\alpha\beta} = \frac{2}{3}\, \mathscr{V}_{\alpha\beta}{}^{-1}\, \mathscr{S}^{*^0}, \qquad \mathscr{V}_{\alpha\beta} = \left[v_{g_{\alpha\beta}}\ \mathbf{J}^T v_{g_{\alpha\beta}}\right],$$
$$i^{*^0}_{\alpha\beta} = \begin{cases} \text{if } \ \|i^{*^0}_{\alpha\beta}\| \le I_N; & \\ \dfrac{I_N}{\|\, i^{*^0}_{\alpha\beta}\|} i^{*^0}_{\alpha\beta}, & \text{if } \ \|\, i^{*^0}_{\alpha\beta}\| > I_N \end{cases} \tag{6}$$

and references recomputed as $[P^*\ \ Q^*]^T = \frac{3}{2}\, \mathscr{V}_{\alpha\beta}\, i^*_{\alpha\beta}$ while powers as $[P\ \ Q]^T = \frac{3}{2}\, \mathscr{V}_{\alpha\beta}\, i_{\alpha\beta}$. PI controllers C_P and C_Q compute virtual control actions ν_P and ν_Q as

$$C_j: \quad \nu_j = K_{p,j}\,(j^* - j) + K_{i,j} \int_0^t (j^* - j) d\tau, \quad j = \{P, Q\}, \tag{7}$$

where $K_{p,j}$ and $K_{i,j}$ are the proportional and integral gains ($j = \{P, Q\}$). Control actions are computed combining the PI feedback terms and feedforward ones as

$$u^0_P = \underbrace{V_g^2 + \frac{2L\omega}{3} Q}_{\text{feedforward}} + \underbrace{\frac{2L}{3}\nu_P}_{\text{feedback}}, \quad u^0_Q = \underbrace{\frac{2L\omega}{3} P}_{\text{feedforward}} - \underbrace{\frac{2L}{3}\nu_Q}_{\text{feedback}}. \tag{8}$$

Here, the saturation of the control action is defined as

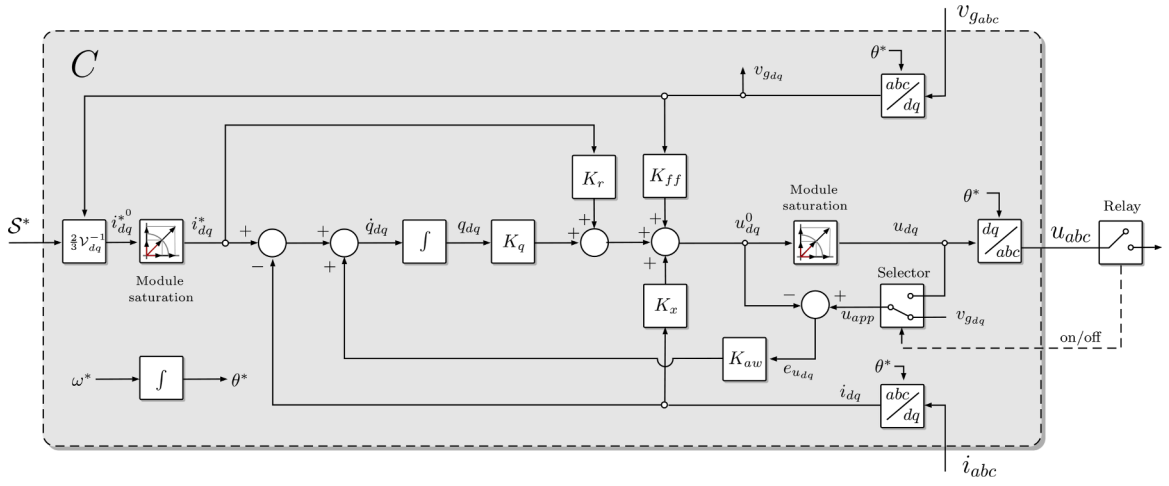

Fig. 4. Proposed MIMO controller block diagram.

$$u_{PQ} = \begin{cases} u^0_{PQ}, & \text{if } \|u^0_{PQ}\| < U^2_{sat}; \\ \dfrac{u^0_{PQ}}{\| u^0_{PQ}\|}\ U^2_{sat}, & \text{if} \| u^0_{PQ} \| > U^2_{sat} \end{cases} \tag{9}$$

and both integral terms of PI controllers are frozen when saturation arises. Finally, control actions $u_{\alpha\beta}$ are restored as $u_{\alpha\beta} = \mathscr{V}^{-1}_{\alpha\beta}\, u_{PQ}$ and an inverse Clarke transformation leads to the voltage u_{abc} to be applied. The design of the PI controllers is done attending the decoupled CL dynamics existing between references and real applied powers (when no saturations arise and assuming stiff grid), that is equivalent to the one in the VCC case (see [16]), leading to

$$\begin{aligned} \frac{P(s)}{P^*(s)} &= \frac{K_{p,P}\, s + K_{i,P}}{s^2 + \left(K_{p,P} + \dfrac{R}{L}\right) s + K_{i,P}}, \\ \frac{Q(s)}{Q^*(s)} &= \frac{K_{p,Q}\, s + K_{i,Q}}{s^2 + \left(K_{p,Q} + \dfrac{R}{L}\right) s + K_{i,Q}}. \end{aligned} \tag{10}$$

3. Proposed approach

Fig. 4 shows a block diagram of the proposed control alternative where the angle θ^* for Clark-Park transformation is obtained integrating $\omega^* = 2\pi f$ (with f the nominal grid frequency, i.e., 50 or 60 Hz), as $\theta^* = \int_0^t \omega^* t$. Then, voltage and current measurements are transformed to the dq frame using θ^*, leading to $v_{g_{dq}}$ and i_{dq} that are of oscillatory nature when ω^* does not fit the grid frequency. Note that we distinguish between two frequencies, namely: (i) grid frequency (ω) and (ii) rotating frequency of the dq frame (ω^*). ω^* is constant whereas ω may change. If we define $\mathscr{S}^* = [P^*\ Q^*]^T$, current references are obtained and limited as in (1). The control action u^0_{dq} is computed as a state feedback control with integral term

$$q_{dq} = \int \left(\left(i^*_{dq} - i_{dq}\right) + K_{aw} \underbrace{\left(u_{app} - u^0_{dq}\right)}_{e_{u_{dq}}} \right) dt, \tag{11a}$$

$$u^0_{dq} = K_r\, i^*_{dq} + K_x\, i_{dq} + K_q\, q_{dq} + K_{ff}\, v_{g_{dq}}, \tag{11b}$$

$$u_{dq} = f\left(u^0_{dq}\right) \text{ as in (4)} \tag{11c}$$

$$u_{app} = \begin{cases} u_{dq}, & \text{if connected;} \\ v_{g_{dq}}, & \text{if not connected} \end{cases} \tag{11d}$$

where u_{app} is the applied control action, q_{dq} the integral of the error $(i^*_{dq} - i_{dq})$ plus the AW term and gain matrices are $\in \mathbb{R}^{2\times 2}$. Matrices K_x and K_q are the proportional and integral gains, K_r weights i^*_{dq} to reduce the overshoot and for improving the behavior under weak grids (we will detail this later) and K_{ff} (identity matrix) is used in the voltage feed-forward term. The saturation mechanism for u_{dq}, as in VCC, keeps the angle of u^0_{dq}. The anti-windup mechanism inspired in [20] is based on including the term $K_{aw}\,(u_{app} - u^0_{dq})$ and its goal is to lead the integral term to a value such that the computed control action u^0_{dq} tracks the real applied one u_{app}, that is equal to the one coming from the controller when the VSC is connected, or equal to the measured grid voltage $v_{g_{dq}}$ in opened situations. In this way, we synchronize the voltages with the ones needed in the grid through the AW mechanism instead of the PLL approach in VCC. Furthermore, by this mechanism we also avoid the windup of the integral term q_{dq} in saturation situations.

3.1. Controller design

For designing the above controller gain matrices, the dynamics in linear operation (with no saturations) and facing stiff grids is used, leading to

$$\dot{\bar{x}} = \mathscr{A}\, \bar{x} + \mathscr{B}_r\, i^*_{dq} + \mathscr{B}_d\, v_{g_{dq}}, \tag{12}$$

where $\mathscr{A} = [[A\ -\mathbf{I}]^T[\mathbf{0}\ \ \mathbf{0}]^T] + \mathscr{B}_u[K_x\ \ K_q]$, $\mathscr{B}_u = [B_u\ \ \mathbf{0}]^T$, $\mathscr{B}_r = [B_u K_r\ \ \mathbf{I}]^T$ and $\mathscr{B}_d = [B_d + B_u K_{ff}\ \ \mathbf{0}]^T$, while $A = -\frac{R}{L}\mathbf{I} - \omega^* \mathbf{J}$, $B_u = \frac{1}{L}\mathbf{I}$ and $B_d = -B_u$. The extended state $\bar{x}$ includes both currents and integral terms: $\bar{x} = [i^T_{dq}\ q^T_{dq}]^T$. This dynamics can be obtained through standard state-space modelling of the grid and matrix manipulations (details omitted for brevity). Matrices K_x, K_q, and K_r can be designed with different techniques like pole placement or optimal control (LQR or H_∞) to achieve a given performance [21].

3.2. Anti-windup design

In saturation conditions (i.e., $u_{dq} \neq u^0_{dq}$) the controller dynamics (11) becomes

$$\begin{aligned} \dot{q}_{dq} &= i^*_{dq} - i_{dq} + K_{aw}\left(u_{app} - u^0_{dq}\right) \\ u^0_{dq} &= K_r\, i^*_{dq} + K_x\, i_{dq} + K_q\, q_{dq} + K_{ff}\, v_{g_{dq}}. \end{aligned}$$

For design purposes, only the internal terms of the controller q_{dq}, u_{app} and u^0_{dq} are considered, assuming null i^*_{dq}, i_{dq} and $v_{g_{dq}}$ without lose of generality. Thus, the computed control action is $u^0_{dq} = K_q\, q_{dq}$, and the dynamics of q_{dq} becomes

$$\dot{q}_{dq} = -K_{aw}\, K_q\, q_{dq} + K_{aw}\, u_{app}. \tag{13}$$

In steady state (i.e., $\dot{q}_{dq} = 0$) and under constant u_{app} it is easy to demonstrate that the computed control action u^0_{dq} fits the applied one u_{app}, i.e., $u^0_{dq} = u_{app}$. From (13) we have that dynamics of q_{dq} depends on the eigenvalues of state matrix $-K_{aw}K_q$. Therefore, once K_q is designed, the anti-windup design reduces to obtain matrix K_{aw}. One can set matrix K_{aw} as $K_{aw} = -\Lambda K_q^{-1}$, defining in that way the dynamics (13) as $\dot{q}_{dq} = \Lambda\, q_{dq}$. Then, the eigenvalues will be defined by the ones in Λ. A common practice is to assign a faster dynamics to this mechanism than the one achieved in closed-loop with the controller by assigning eigenvalues in Λ with a real part larger than the one in $\mathscr{A}$ in (12)

3.3. Comparison with VCC and GVM-DPC approaches

Table 1 shows a comparison of the proposed control strategy and the VCC and DPC regarding the next criteria: C1, use of a PLL; C2, decoupling mechanism; C3, current limitation mechanism; C4, control action saturation mechanism; C5, anti-windup mechanism; C6, degrees of freedom.

In VCC and DPC, under a fixed grid frequency that fits the one used in

Table 1
Comparison of the different control approaches.

	C1	C2	C3	C4	C5	C6
VCC	Yes	$-L\omega i_d$, $L\omega i_q$	$\| i^*_{dq}\| < I_N$	$\| u^0_{dq}\| < U_{sat}$	Standard	K_{p,i_d}, K_{i,i_d}, K_{p,i_q}, $K_{i,i_q} \in \mathbb{R}$
DPC	No	$2/3\, L\omega Q$, $2/3\, L\omega P$	Modifying P^* and Q^*	$\| u^0_{PQ}\| < U^2_{sat}$	Standard	$K_{p,P}$, $K_{i,P}$, $K_{p,Q}$, $K_{i,Q} \in \mathbb{R}$
MIMO	No	No	$\| i^*_{dq}\| < I_N$	$\| u^0_{dq}\| < U_{sat}$	MIMO anti-windup	K_r, K_x, K_q, K_{ff}, $K_{aw} \in \mathbb{R}^{2\times 2}$

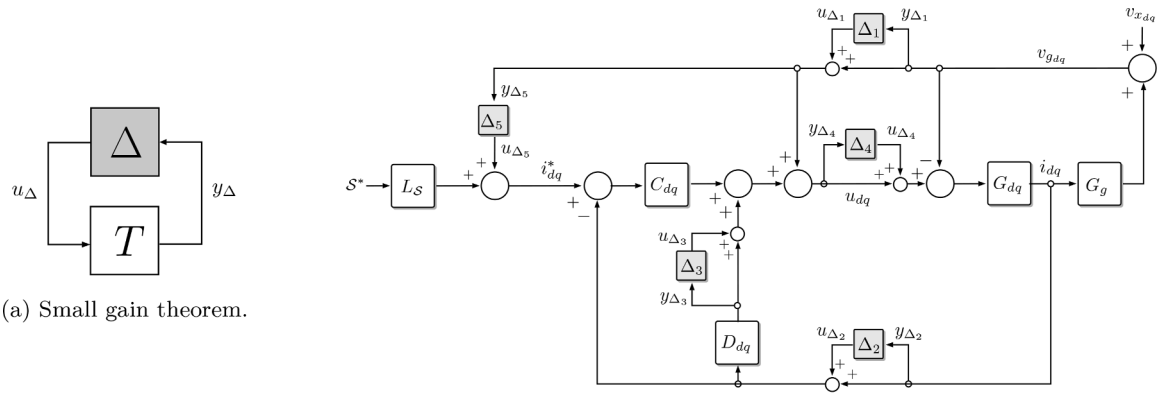

(a) Small gain theorem.

(b) VCC approach block diagram in a weak grid.

Fig. 5. Small gain theorem modelling needs and application to VCC.

Table 2
Interconnection transfer matrices in weak grid analysis.

	VCC	DPC	MIMO
T_{Δ_1}	$G_g S_{dq} G_{dq}$	$G_g^T S_\mathcal{J} G_\mathcal{J}$	$G_g S_p G_p$
T_{Δ_2}	$S_{dq} G_{dq} (D_{dq} - C_{dq})$	$S_\mathcal{J} G_\mathcal{J} (D_\mathcal{J} - C_\mathcal{J})$	$S_p G_p C_i$
T_{Δ_3}	$D_{dq} S_{dq} G_{dq}$	$D_\mathcal{J} S_\mathcal{J} G_\mathcal{J}$	-
T_{Δ_4}	$(G_g + D_{dq} - C_{dq}) S_{dq} G_{dq}$	$(G_g^T + D_\mathcal{J} - C_\mathcal{J}) S_\mathcal{J} G_\mathcal{J}$	$(G_g + C_i) S_p G_p$
T_{Δ_5}	$G_g S_{dq} G_{dq} C_{dq}$	$G_g^T S_\mathcal{J} G_\mathcal{J} (D_\mathcal{J} - C_\mathcal{J})$	$G_g S_p G_p C_{i^*}$

the decouplers, the references and disturbances can be considered almost constant in their frames. However, in our approach, as the internal frequency ω^* may not fit the grid one ω, the references and disturbances present a persistent oscillatory nature of frequency equal to difference $\omega - \omega^*$ (typically few mHz). This is something that our controller must tackle from the design phase.

4. Robustness analysis under weak grids

If we have a feedback system as in Fig. 5a, where $T(s)$ and $\Delta(s)$ are two LTI stable systems, by using the small gain theorem we have that the feedback system will be stable if $\sup_{\omega\in\mathbb{R}} \overline{\sigma}(\Delta(j\omega))\overline{\sigma}(T(j\omega)) < 1$ (where $\overline{\sigma}(\cdot)$ denotes maximum singular value of the frequency response). This indicates that a frequency-by-frequency fulfilment is sufficient to assure stability, so the frequency response of T^{-1} gives us information on the allowed uncertainties that the loop can afford before becoming unstable [21]. For the stability analysis we model the following uncertainty sources for each of the three alternative power control techniques:

Δ_1: Errors in voltages measurements due to PLL and delays.
Δ_2: Errors in currents measurements due to PLL and delays.
Δ_3: Errors in decoupling terms due to the use of a constant ω value.
Δ_4: Errors in control action construction due to PWM.
Δ_5: WG induced feedback channel changing current references

To establish the robustness implication of each uncertainty source, we must obtain the transfer function that expresses its effect on the system behaviour (T in Fig. 5a). To achieve that, we present a block diagram for each of the strategies that incorporates the mentioned uncertainties, and we point at the signals u_{Δ_i} and y_{Δ_i} (as in Fig. 5a) needed to obtain the corresponding T_{Δ_i} transfer function.

When obtaining the transfer function we take into account the short circuit capacity S_{cc} of the grid (modelled with L_g in Fig. 1). With this, we can identify the limits of each strategy in weak grids. Hence, frequencies at which the values of $\overline{\sigma}(T_{\Delta_i}(j\omega))$ are higher, imply that the uncertainty Δ_i at those frequencies should be lower to guarantee stability. On the other hand, if the frequency range where the uncertainty may appear is known and bounded, $\overline{\sigma}(T_{\Delta_i}(j\omega))$ at that range should be lower than the inverse of the uncertainty. In the sequel, block diagram and matrix manipulation details to derive T_{Δ_i} are omitted for space constraints.

Fig. 5 b includes the considered uncertainties for the case of VCC control, while the resulting transfer functions that model the uncertainty interactions are shown in Table 2, where $S_{dq} = (\mathbf{I} + G_{dq}(C_{dq} - D_{dq}))^{-1}$,

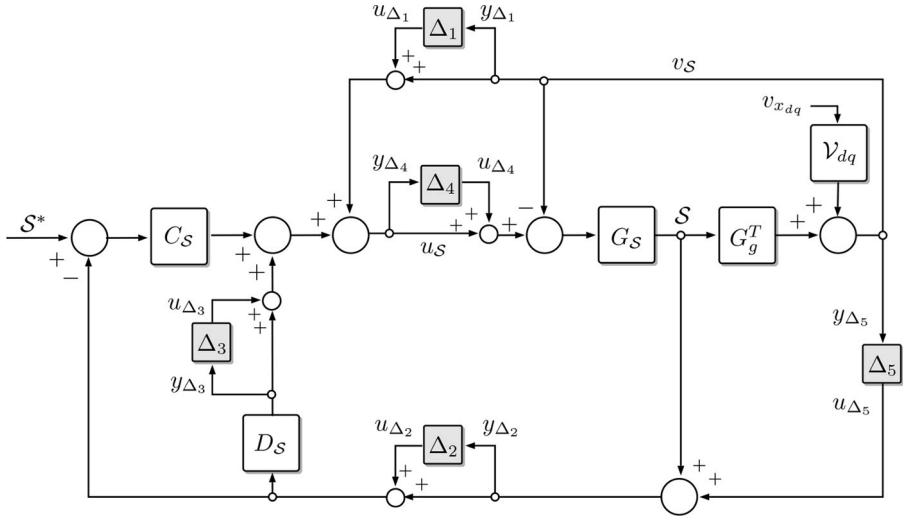

Fig. 6. GVM-DPC approach block diagram in a weak grid.

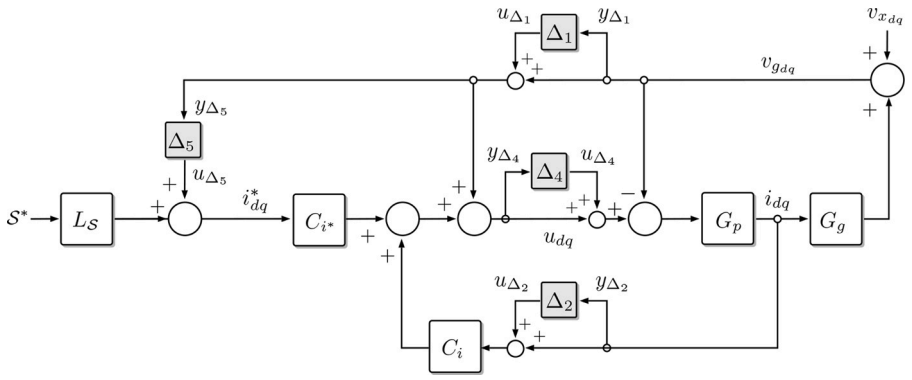

Fig. 7. MIMO proposal block diagram in a weak grid.

being G_{dq} and G_g the transfer function matrices that model the converter and grid behaviours

$$G_{dq} = \frac{\frac{1}{L}}{s^2 + 2\frac{R}{L}s + \omega^2 + \frac{R^2}{L^2}}\left(\left(s + \frac{R}{L}\right)\mathbf{I} - \omega\mathbf{J}\right),$$
$$G_g = L_g\,(s\mathbf{I} + \omega\mathbf{J}),$$

and C_{dq} and D_{dq} those matrices related to the PI controllers and decoupling terms

$$C_{dq} = L\begin{bmatrix} K_{p,i_d} + \frac{1}{s}K_{i,i_d} & 0 \\ 0 & K_{p,i_q} + \frac{1}{s}K_{i,i_q} \end{bmatrix},$$
$$D_{dq} = L\omega\mathbf{J}.$$

Fig. 6 includes the considered uncertainties for the case of GVM-DPC control, while the uncertainty interactions are shown in Table 2, where $S_{\mathscr{J}} = (\mathbf{I} + G_{\mathscr{J}}(C_{\mathscr{J}} - D_{\mathscr{J}}))^{-1}$ being $G_{\mathscr{J}}$ and G_g the transfer matrices that model the converter and the grid

$$G_{\mathscr{J}} = \frac{\frac{3}{2L}}{s^2 + 2\frac{R}{L}s + \omega^2 + \frac{R^2}{L^2}}\begin{bmatrix} s + \frac{R}{L} & \omega \\ \omega & -\left(s + \frac{R}{L}\right) \end{bmatrix},$$
$$G_g = L_g\,(s\mathbf{I} + \omega\mathbf{J}),$$

and $C_{\mathscr{J}}$ and $D_{\mathscr{J}}$ those matrices modelling the PI controllers and decoupling terms

$$C_{\mathscr{J}} = \frac{2L}{3}\begin{bmatrix} K_{p,P} + \frac{1}{s}K_{i,P} & 0 \\ 0 & -\left(K_{p,Q} + \frac{1}{s}K_{i,Q}\right) \end{bmatrix},$$
$$D_{\mathscr{J}} = \frac{2L}{3}\begin{bmatrix} 0 & \omega \\ \omega & 0 \end{bmatrix}.$$

Fig. 7 includes the considered uncertainties for the case of MIMO control, while Table 2 shows the resulting interactions, with $S_p = (\mathbf{I} - G_pC_i)^{-1}$ being G_p and G_g the transfer function matrices that model the converter and grid behaviours

$$G_p = \frac{\frac{1}{L}}{s^2 + 2\frac{R}{L}s + \omega^{*2} + \frac{R^2}{L^2}}\left(\left(s + \frac{R}{L}\right)\mathbf{I} - \omega^*\mathbf{J}\right),$$
$$G_g = L_g\,(s\mathbf{I} + \omega\mathbf{J}).$$

Table 3
Parameters used in simulations.

Parameter	Value	Parameter	Value
VSC nominal power	2 kVA	Nominal frequency f	50 Hz
Nominal grid voltage (rms)	110 V	Voltage saturation U_{sat}	1.2 p.u.
Resistance R	0.2 Ω (0.011 p. u.)	Rated current I_N	1 p.u.
Inductance L	5 mH (0.08 p.u.)		

and C_{i^*} and C_i those transfer function matrices modelling the MIMO controller

$$C_{i^*} = K_r + \frac{1}{s}K_q, \qquad C_i = -\left(K_x + \frac{1}{s}K_q\right).$$

5. Simulation results

VCC, GVM-DPC and MIMO proposal are compared in this section by means of MATLAB/Simulink simulations. System parameters are shown in Table 3 [16]:

PI controllers are designed with CL poles $-400 \pm 400j$ leading to

$$K_p = 760, \quad K_i = 3.2{\cdot}10^5,$$

where $K_p = K_{p,i_d} = K_{p,i_q} = K_{p,P} = K_{p,Q}$ and $K_i = K_{i,i_d} = K_{i,i_q} = K_{i,P} = K_{i,Q}$. MIMO controller has been designed first to have the same poles and zeros than VCC and GVM-DPC, leading to controller MIMO$_1$ defined by

$$K_x = L\big(-K_p\mathbf{I} + \omega^*\mathbf{J}\big) = -3.8\,\mathbf{I} + 1.57\,\mathbf{J},$$
$$K_q = L\,K_i\,\mathbf{I} = 1600\,\mathbf{I},$$
$$K_r = L\,K_p\,\mathbf{I} = 3.8\,\mathbf{I}$$

The anti-windup has been designed to be 5 times faster than the CL behaviour leading to $K_{aw} = 1.25\,\mathbf{I}$. We have also designed other MIMO controllers (number 2 and 3) by using only a different matrix K_r (♯2: $K_r = 1.9\,\mathbf{I}$, ♯3: $K_r = \mathbf{0}$).

S1: Tracking power references

Fig. 8 a shows the behaviour of the five control approaches for tracking power references showing a settling time of 10 ms. Decoupling terms in the control laws in VCC and GVM-DPC or the proposed MIMO approach itself make the controlled system behave decoupled. As the first three controllers have been designed for having the same CL poles, their time responses appear superimposed. The last two controllers show a lower overshoot due to a lower value in K_r.

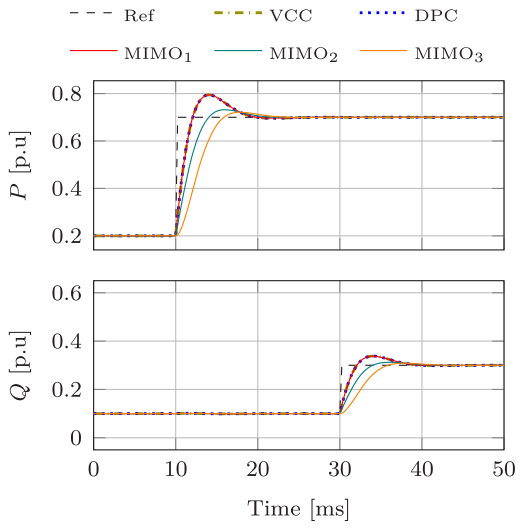

(a) Power references tracking.

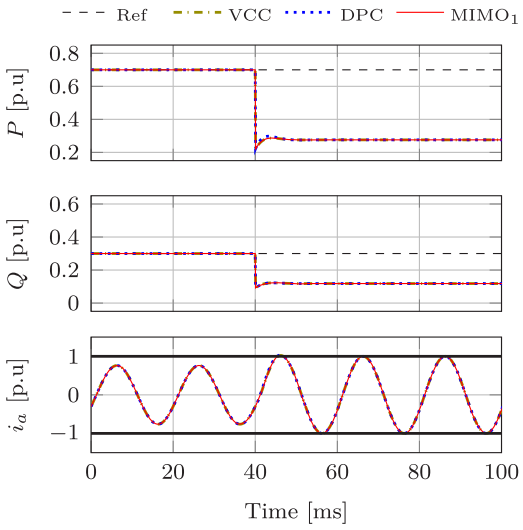

(b) Grid voltage sag of 70% .

Fig. 8. Behavior tracking power references (a) and facing a voltage sag of 70% (b).

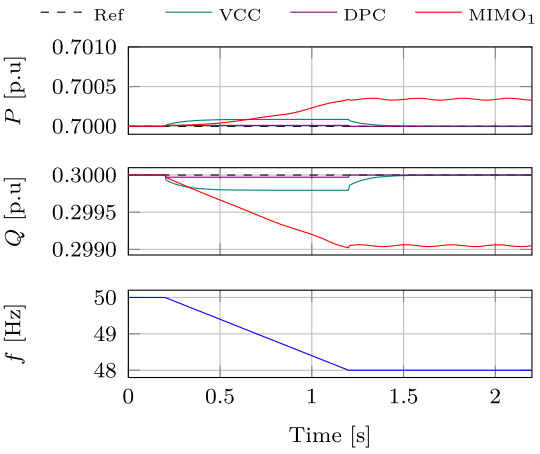

(a) Power reference tracking.

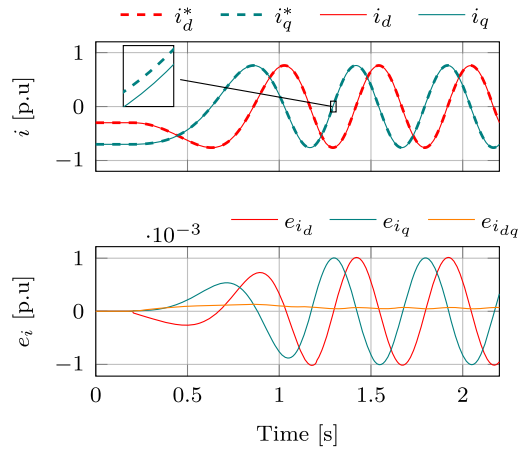

(b) Current reference traking of $MIMO_1$.

Fig. 9. Power and current tracking when there are frequency deviations.

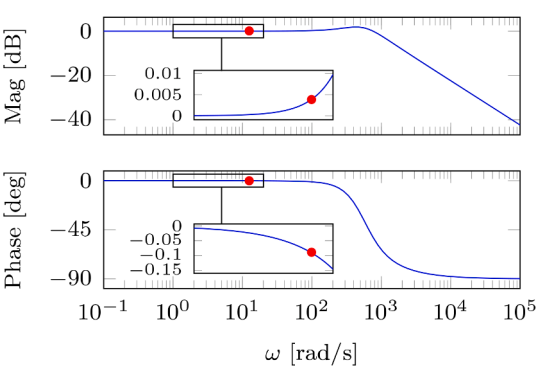

(a) Bode diagram of closed loop transfer function from i^*_{dq} to i_{dq}.

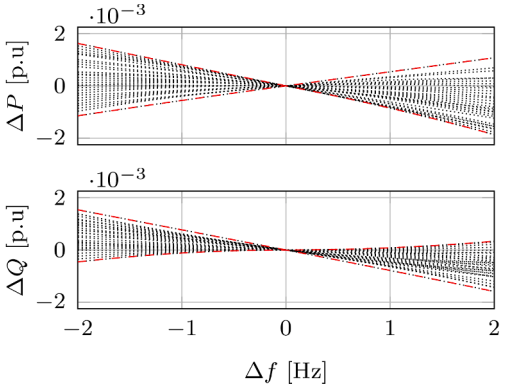

(b) Steady state errors in tracking power references for different grid frequency deviations of $MIMO_1$.

Fig. 10. Errors due to grid voltage deviations.

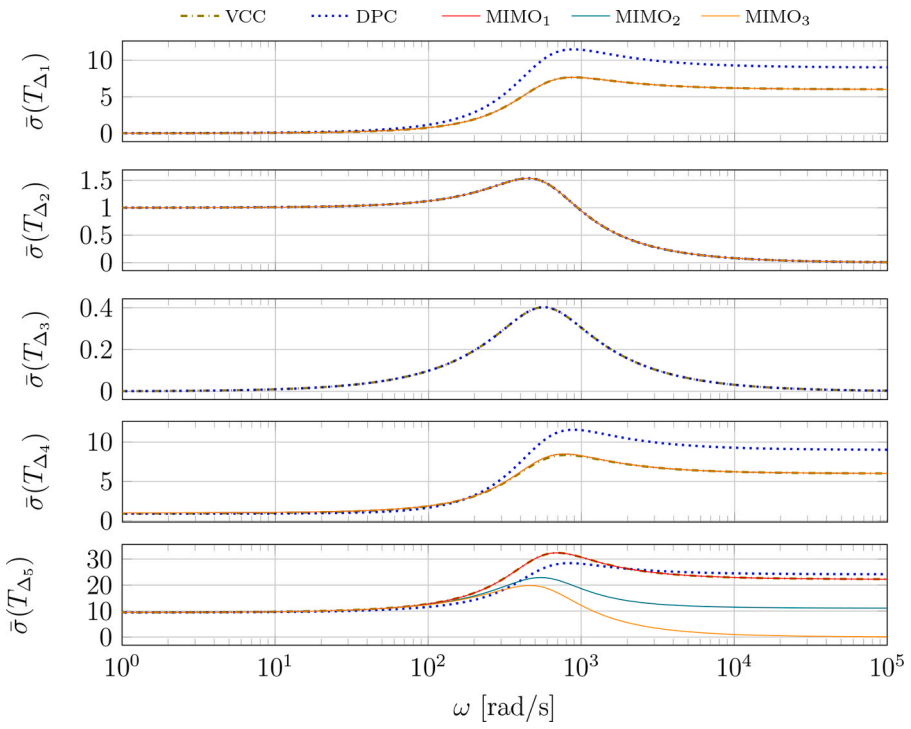

Fig. 11. Maximum singular values of T_{Δ_i}.

S2: Voltage sag (70%)

Fig. 8 b shows the behaviour of the three control approaches (VCC, DPC and MIMO$_1$) when at time $t = 40$ ms the grid has a voltage sag of 70%, i.e., the magnitude of the grid voltage drops from 1 to 0.3 p.u. It can be seen that all approaches lose the control of both, active and reactive powers, but all of them have an effective current limitation as a protection mechanism. Time responses appear almost superimposed and currents remain smaller than 1 p.u. (in absolute value).

S3: Frequency deviations

Fig. 9 a shows the behaviour of the first three control approaches when, at time $t = 0.1$ s, there is a change of 2 Hz in the grid frequency from the nominal value of 50 Hz to 48 Hz with a rate of change of frequency (RoCoF) of 2 Hz/s. Although it is a much larger frequency deviation that a power grid will experience, it allows to compare the three control strategies. GVM-DPC approach shows the fastest transient response with the minimum error. VCC has a slower transient response because of the use of the PLL, thus, its performance depends on the PLL design. Both alternatives has no steady-state error. Finally, the MIMO$_1$ proposal presents some steady-state error (less than 0.002 p.u.). When there is a deviation between the real grid voltage frequency and the fixed one used by the converters, the current references i^*_{dq} are not constant signals but they are sinusoidal ones of frequency equal to the difference between the real frequency and the nominal one used by converters for doing the Clarke-Park transformations. Similarly, u_d and u_q are also sinusoidal signals of the same (slow) frequency (only 2 Hz). The MIMO and PI controllers can track constant references but not sinusoidal ones with null steady state error. As it is shown in Fig. 9b there exist little errors that we will measure as $e_{i_d} = i^*_d - i_d$, $e_{i_q} = i^*_q - i_q$ and $e_{i_{dq}} = \| i^*_{dq}\| - \| i_{dq}\|$. The magnitude of steady state errors when there are deviations in grid frequency from its nominal value depends on the controller design. The faster is the controller, the smaller is the steady-state error. The tracking error will depend on the frequency response of the CL transfer function from i^*_d to i_d evaluated at the frequency deviation. Fig. 10a shows the Bode diagram of that transfer function and we see that,both, magnitude and phase errors are negligible for the possible common frequency deviations.

For this particular case, Fig. 10b shows steady state errors ΔP and ΔQ in tracking active and reactive powers for different values of the deviations in the grid frequency Δf and for different operation points (i.e., different combinations of P^* and Q^*). As we can see, in the worst case, these errors are smaller than 0.002 p.u. Moreover, for grid-connected converters, frequency deviations with respect to the rated frequency are usually much more smaller than 2Hz, usually only a few miliherzts. For instance, for a deviation of 100 mH, power reference tracking errors are smaller than 10^{-4} p.u and it could be avoided with an outer power control loop [17]. These errors are comparable to the ones obtained when a stationary frame along with proportional-resonant (PR) controllers are used. Given that PR controllers are designed to track references at a specific frequency, there will also be a current tracking error in case of grid frequency deviations.

S4: Weak grid

We test now the five controllers in a WG simulated with the grid impedance $L_g = 0.5$ p.u., and the short-circuit ratio is $SCR = 2$. For the robustness analysis, we assume that the PLL in VCC implies an error in the measurement of the frequency in the order of $10^2 - 10^3$ $\frac{rad}{s}$, the delays in measurements errors in the frequency range of the sampling frequency, normally in the order of 10^5 $\frac{rad}{s}$, and the delays for voltage reconstruction in the PWM, in the order of 10^4 $\frac{rad}{s}$.

Fig. 11 shows the maximum singular values $\bar{\sigma}$ of the frequency response of the transfer functions T_{Δ_i} $(i = \{1, \ldots, 5\})$ for the five controllers.

The first thing to notice is that the VCC strategy, and the MIMO$_1$ present the same frequency response for all uncertainties. The technique of DPC has also the same frequency response against uncertainty channels 2 and 3, but differs in the others. This difference is due to the uncertainty channel included in the analysis, that refers to variations on the square of the voltage instead of the voltage itself.

From the plots that show $\bar{\sigma}(T_{\Delta_1})$ and $\bar{\sigma}(T_{\Delta_2})$ in Fig. 11 we notice that all the techniques support better high frequency measurement errors (due to delays) than middle frequency ranges (in the order of 10^3 $\frac{rad}{s}$). This is where one notices that the VCC can become unstable due to the

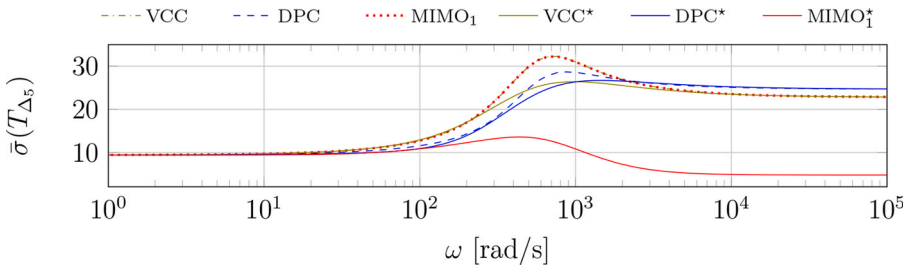

Fig. 12. Comparison of $\overline{\sigma}(T_{\Delta_5})$ for original and optimized controllers.

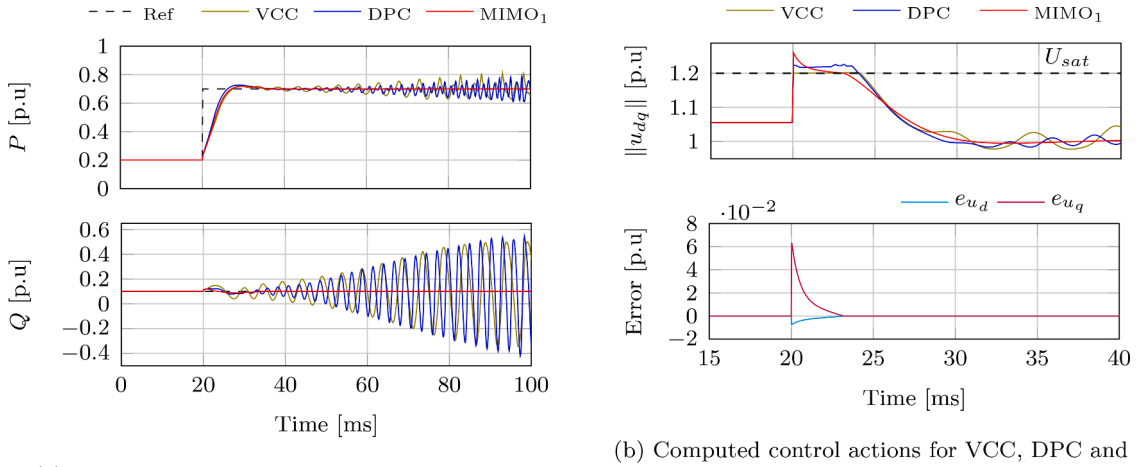

(a) Power references tracking in a weak grid.

(b) Computed control actions for VCC, DPC and MIMO$_1$ and errors $e_{u_{dq}}$ for MIMO$_1$.

Fig. 13. Step change in P^* when VSC is connected to a weak grid with SCR=2.

use of the PLL as, at that frequency, only errors in the order of 10% will be allowed.

From the plots that show $\overline{\sigma}(T_{\Delta_3})$ in Fig. 11 we see that the uncertainty associated to the decoupler has low values in the singular value plot, meaning that this is not a main source of instability. However, the frequencies in which the effect is most amplified is in the order of 10^3 $\frac{rad}{s}$. One may have that error if the grid frequency value used in the decouplers is computed from the one obtained in the PLL. This suggests to avoid the use of the measured ω in the decoupling terms in control techniques VCC and DPC, and, instead, use a nominal constant value.

From plot that show $\overline{\sigma}(T_{\Delta_4})$ in Fig. 11 we see that PWM voltage reconstruction can be a problem that destabilizes the loop in VCC technique. The faster frequencies related to the PWM affect in an equivalent way to all the techniques.

The feedback channel through uncertainty Δ_5 and quantified in the bottom graph of Fig. 11 shows that in the case of VCC and MIMO$_1$, it can accept a feedback with maximum static gain in the order of 1/9.4=0.106. We have seen, for instance, in the VCC case, that this feedback channel has static gains in the order of $\frac{2\overline{P}}{3V_g^2} \in [0, 0.055]$ (depending on the operation point) and, thus, the system will remain stable. Finally, we see that using lower values in matrix K_r (controllers MIMO$_2$ and MIMO$_3$) allows increasing the allowable Δ_5 uncertainty, thus, improving the behavior under weak grids. We see also that the value of K_r does not affect the rest of uncertainty channels.

In order to focus the controllers design on facing weak grids, we can obtain the gains through the following optimization procedure

$$\underset{K}{\text{minimize}}\ \max\overline{\sigma}(T_{\Delta_5}); \quad \text{subject to: } \max\Re\mathrm{e}(\lambda_i) < -400,$$

where K refers to the controller gains of each approach, and where we have fixed the same real part of the poles as in the initial controllers for comparison. With this, the optimized PI controllers for operating in a weak grid with SCR=2 are defined by $K_p = 760$ and $K_i = 1.6\,10^5$ for VCC and GVM-DPC approaches and by

$$K_x = \begin{bmatrix} 5.3443 & 2.3673 \\ -1.5829 & 5.4379 \end{bmatrix},$$

$$K_q = \begin{bmatrix} 1600 & 11 \\ 3 & 1600 \end{bmatrix},$$

$$K_r = \begin{bmatrix} 0.079 & 0.7471 \\ 0.6913 & 0.079 \end{bmatrix},.$$

for MIMO proposal. Fig. 12 shows the frequency response of T_{Δ_5}, where we appreciate lower magnitude, showing a better performance when facing weak grids. We see that the highest robustness is achieved by means of the MIMO approach, thanks to have more degrees of freedom.

In this situation, saturation and anti-windup mechanisms come into play (Fig. 13b). In particular, the bottomed graph shows that the errors between applied and computed control actions $e_{u_d} = u_d - u_d^0$ and $e_{u_q} = u_q - u_q^0$ go to zero in 2 ms, i.e., 5 times faster than current controller. Fig. 13a shows the behavior of the first three controllers for $SCR = 2$ when a step change in P^* is produced. As it is shown, VCC and GVM-DPC methods become unstable while our MIMO$_1$ not.

6. Conclusions

In this work, we have proposed a multivariable (MIMO) control strategy for power control of grid-connected VSC without using a PLL, and, thus, avoiding the dynamic interaction that appears in weak grids. We face our control problem in a *dq* frame, and avoiding the PLL generates internal oscillating signals that our controller tackles thanks to having extra degrees of freedom w.r.t. standard PI plus decoupling

control. Futhermore, we include reference weighting factors that help us to face weaker grids w.r.t. VCC and GVM-DPC. We also include an AW mechanism that avoids the problems of other standard approaches when extended to PI control with decouplers (as in VCC or GVM-DPC), and that also faces the synchronization in the absence of a PLL. With a small gain theorem based approach we have analysed the different uncertainties that may lead to instabilities, and has also helped us to demonstrate our improvement when facing weak grids.

CRediT authorship contribution statement

Carlos Diaz-Sanahuja: Writing – original draft, Writing – review & editing, Software, Investigation, Methodology, Conceptualization, Formal analysis. **Ignacio Peñarrocha-Alós:** Writing – original draft, Writing – review & editing, Supervision, Formal analysis, Conceptualization. **Ricardo Vidal-Albalate:** Writing – original draft, Writing – review & editing, Supervision, Conceptualization.

Declaration of Competing Interest

The authors declare that they have no known competing financial interests or personal relationships that could have appeared to influence the work reported in this paper.

Acknowledgments

The present work was supported by the Spanish Ministry of Science, Innovation and Universities (Grant FPU16/03505).The authors would also like to thank the Spanish Research Agency for their help through grant PID2020-112943RB-I00 funded by MCIN/AEI/10.13039/501100011033 and grant PDC2021-121077-I00.

References

[1] S. Peyghami, P. Palensky, F. Blaabjerg, An overview on the reliability of modern power electronic based power systems, IEEE Open J. Power Electron. 1 (2020) 34–50.
[2] S. Ansari, A. Chandel, M. Tariq, A comprehensive review on power converters control and control strategies of AC/DC microgrid, IEEE Access 9 (2021) 17998–18015.
[3] Z. Li, C. Zang, P. Zeng, H. Yu, S. Li, J. Bian, Control of a grid-forming inverter based on sliding-mode and mixed H_2/H_∞ control, IEEE Trans. Ind. Electron. 64 (5) (2017) 3862–3872.
[4] X. Wang, L. Harnefors, F. Blaabjerg, Unified impedance model of grid-connected voltage-source converters, IEEE Trans. Power Electron. 33 (2) (2018) 1775–1787.
[5] H. Gong, X. Wang, L. Harnefors, Rethinking current controller design for pll-synchronized vscs in weak grids, IEEE Trans. Power Electron. 37 (2) (2022) 1369–1381.
[6] B. Wen, D. Boroyevich, R. Burgos, P. Mattavelli, Z. Shen, Analysis of d-q small-signal impedance of grid-tied inverters, IEEE Trans. Power Electron. 31 (1) (2016) 675–687.
[7] X. Wang, F. Blaabjerg, Harmonic stability in power electronic-based power systems: Concept, modeling, and analysis, IEEE Trans. Smart Grid 10 (3) (2019) 2858–2870.
[8] A. Tarraso, L. Marin, N.B. Lai, P. Rodriguez, Enhanced Proportional-Resonant (PR) Controller with Negative Decoupling for Weak Grids. IEEE 21st Workshop on Control and Modeling for Power Electronics (COMPEL), 2020, pp. 1–4.Aalborg, Denmark
[9] J.F. Morris, K.H. Ahmed, A. Egea-Alvarez, Power-synchronization control for ultra-weak AC networks: comprehensive stability and dynamic performance assessment, IEEE Open J. Ind. Electron. Soc. 2 (2021) 441–450.
[10] A. Rodriguez-Cabero, J. Roldan-Perez, M. Prodanovic, Virtual impedance design considerations for virtual synchronous machines in weak grids, IEEE Trans. Emerg. Sel. Top. Power Electron. 8 (2) (2020) 1477–1489.
[11] J. Roldan-Perez, A. Rodriguez-Cabero, M. Prodanovic, Design and analysis of virtual synchronous machines in inductive and resistive weak grids, IEEE Trans. Energy Convers. 34 (4) (2019) 1818–1828.
[12] L. Shang, J. Hu, Sliding-mode-based direct power control of grid-connected wind-turbine-driven doubly fed induction generators under unbalanced grid voltage conditions, IEEE Trans.Energy Convers. 27 (2) (2012) 362–373.
[13] C.A. Alfaro Aragon, R. Guzman, L.G. De Vicuna, H. Komurcugil, H. Martin, Distributed Direct Power Sliding-Mode Control for Islanded AC Microgrids, IEEE Trans. Ind. Electron. (2021).Early Access
[14] Y. Gui, G.H. Lee, C. Kim, C.C. Chung, Direct power control of grid connected voltage source inverters using port-controlled hamiltonian system, Int. J. Control Autom. Syst. 15 (5) (2017) 2053–2062.
[15] Y. Gui, X. Wang, F. Blaabjerg, Vector current control derived from direct power control for grid-connected inverters, IEEE Trans. Power Electron. 34 (9) (2019) 9224–9235.
[16] Y. Gui, X. Wang, F. Blaabjerg, D. Pan, Control of grid-connected voltage-source converters: The relationship between direct-power control and vector-current control, IEEE Ind. Electron. Mag. 13 (2) (2019) 31–40.
[17] W. Wang, A. Beddard, M. Barnes, O. Marjanovic, Analysis of active power control for vschvdc, IEEE Trans. Power Deliv. 29 (4) (2014) 1978–1988.
[18] Z. Ali, N. Christofides, L. Hadjidemetriou, E. Kyriakides, Y. Yang, F. Blaabjerg, Three-phase phase-locked loop synchronization algorithms for grid-connected renewable energy systems: a review, Renew. Sustain. Energy Rev. 90 (2018) 434–452.
[19] L. Harnefors, H.P. Nee, Model-based current control of ac machines using the internal model control method, IEEE Trans. Ind. Appl. 34 (1) (1998) 133–141.
[20] U. Christen, H.P. Geering, Anti-windup for mimo controllers, IFAC Proceedings Volumes 29 (1) (1996) 1536–1541.13th World Congress of IFAC, 1996, San Francisco USA, 30 June - 5 July
[21] P. Albertos, S. Antonio. Multivariable Control Systems: an Engineering Approach, Springer Science & Business Media, 2006.